Materials Today Bio 32 (2025) 101736

Contents lists available at ScienceDirect

Materials Today Bio

journal homepage: www.journals.elsevier.com/materials-today-bio

Application of a novel thermal/pH-responsive antibacterial paeoniflorin hydrogel crosslinked with amino acids for accelerated diabetic foot ulcers healing

Xintao Jia [a,b,c,d,1], Zixuan Dou [b,c,d,1], Ying Zhang [b,c,d], Changxiang Yu [a,b,c,d], Mengru Yang [a,b,c,d], Haonan Xie [a,b,c,d], Yun Lin [a,b,c,d], Zhidong Liu [a,b,c,d,*]

[a] School of Chinese Materia Medica, Tianjin University of Traditional Chinese Medicine, Tianjin, 301617, China
[b] State Key Laboratory of Component Based Chinese Medicine, Tianjin University of Traditional Chinese Medicine, Tianjin, 301617, China
[c] Engineering Research Center of Modern Chinese Medicine Discovery and Preparation Technique, Ministry of Education, Tianjin University of Traditional Chinese Medicine, Tianjin, 301617, China
[d] Haihe Laboratory of Modern Chinese Medicine, Tianjin, 301617, China

ARTICLE INFO

Keywords:
Diabetic foot ulcers
Amino acids
Wound dressing
Crosslinker
Paeoniflorin

ABSTRACT

Diabetic foot ulcers (DFUs), a severe and common complication of diabetes, present significant treatment challenges due to the limitations of conventional dressings, such as poor mechanical properties, bioactivity, and limited functionality, which hinder fast and effective wound healing. To address these issues, we developed a novel natural amino acid-based hydrogel loaded with paeoniflorin (PF@PNMA1) and comprehensively evaluated its properties and functions. The nanogel particles (NGs) were synthesized via emulsion polymerization using N-isopropylacrylamide (NIPAM), methacrylic acid (MAA), and chemically modified arginine (MArg). The poly (NIPAM-co-MAA) (PNM) and poly(NIPAM-co-MAA-co-MArg) (PNMA) gels were prepared by functionalizing the NGs with glycidyl methacrylate (GMA). The different concentrations of amino acids were added to explore the optimal mechanical properties of the gel. Through the rheological measurement, we found that PNMA1 gel has good ductile properties with a critical strain up to about 63 %. At the same time, we also verified its antibacterial activity and found that the viability of bacteria decreased to 47.46 % after 3 h. Preliminary tests using network pharmacology and molecular docking confirmed the therapeutic potential of PF for DFUs. The PF@PNMA1 gel demonstrated excellent biocompatibility, and in vivo experiments revealed its effectiveness in promoting angiogenesis and wound healing. After 10 days, the wound healing rate was 25.6 % higher than that of the control group. The PF@PNMA1 shows great potential as an effective therapy for DFUs treatment.

1. Introduction

Diabetic foot ulcers (DFUs) are a serious complication of diabetes and pose a significant medical challenge, affecting 40 to 60 million individuals worldwide [1]. The emergence of a globally aging population has intensified the therapeutic challenges associated with DFUs. These wounds are difficult to heal and present a high risk of infection. In severe cases, DFUs may lead to amputations [2,3]. The primary etiological factors contributing to DFUs include persistent hyperglycemia-induced vasculopathy and neuropathy. In addition, the pathological characteristics of diabetic wounds involve excessive inflammatory responses, and bacterial infections further exacerbate the wound microenvironment [4,5]. Traditional treatments usually involve dressings and topical medications to manage wounds, prevent infection, and promote healing. However, conventional dressings face several challenges, including inadequate moisture retention, inefficient delivery of bioactive substances, and limited adaptability to the wound's complex environment. These limitations underscore the need for more advanced dressings.

Hydrogels have emerged as a promising dressing due to their better

* Corresponding author. School of Chinese Materia Medica, Tianjin University of Traditional Chinese Medicine, Tianjin, 301617, China.
E-mail addresses: lonerliuzd@163.com, liuzhidong@tjutcm.edu.cn (Z. Liu).
[1] These authors have contributed equally to this work and share first authorship.

https://doi.org/10.1016/j.mtbio.2025.101736
Received 3 January 2025; Received in revised form 1 April 2025; Accepted 5 April 2025
Available online 5 April 2025

moisture control, enhanced drug delivery, and a more adaptable structure, making them a promising alternative for DFUs treatment. Because of their three-dimensional (3D) hydrophilic polymer network, the water content more than 70 % [6]. They can maintain a moist environment at the wound site and exhibit excellent biocompatibility. Their mechanical properties can be adjusted, and they closely resemble the extracellular matrix, fostering the recovery of skin tissues [7]. Hydrogels can be utilized in a variety of ways to obtain a variety of functions, such as antibacterial [8], anti-inflammatory [9–11], and responsive properties [12]. It is essential to emphasize that hydrogels used for wound treatment must possess adequate mechanical properties and efficient drug-carrying capacity. Therefore, the selection of hydrogel monomers, cross-linking agents, and reaction conditions is critical. Notably, some cross-linking agents can be potentially toxic, and finding ways to minimize their use while still effectively regulating the properties of hydrogels presents a significant challenge. It has been reported that proteins, peptide fragments, and specific amino acids can influence the mechanical properties, rheological behavior, and degradation rate of hydrogels [13,14]. Furthermore, the natural presence of proteins and amino acids in the body ensures their excellent biocompatibility, thereby minimizing the risk of toxicity and adverse reactions when incorporated into drug delivery systems. For example, a new type of gel cross-linked with tethered antibacterial cationic polyimidazolium and antioxidative *N*-acetylcysteine has been reported, with *N*-acetylcysteine promoting keratinocyte differentiation and accelerating the reepithelialization process [15].

Arginine, an essential amino acid with a basic guanidine chain, plays a crucial role in various physiological functions [16–19]. The functional groups present in arginine allow for fine-tuning the properties of polymers, including mechanical strength [20]. In addition, in the healing process of diabetic foot wounds, antibacterial action is crucial to prevent infections and promote tissue regeneration. For example, certain hydrogels loaded with antibacterial agents like silver nanoparticles, antibiotics have been shown to effectively reduce bacterial growth [21–23]. The intrinsic antibacterial capacity of arginine enables the hydrogel dressing to facilitate enhanced wound healing. Therefore, we chose to introduce natural arginine as a crosslinker into the gels. To optimize the bioavailability of L-arginine at the wound site, we chemically modified it to create an amphoteric monomer, modified arginine (MArg).

We combine MArg with *N*-isopropylacrylamide (NIPAM) and methacrylic acid (MAA) through emulsion polymerization. NIPAM is known for its thermoresponsive properties, as it undergoes a reversible phase transition in response to temperature changes. Below its lower critical solution temperature (LCST), it swells and becomes hydrophilic, while above the LCST, it becomes hydrophobic and shrinks. Methacrylic acid, provides pH -responsive property due to its ionizable carboxyl groups. At low pH, MAA remains protonated and hydrophobic, while at higher pH levels, the carboxyl groups deprotonate, making the polymer more hydrophilic and promoting swelling. Therefore, by controlling the ratio of arginine, as well as the temperature and pH, the properties of the hydrogel can be precisely tuned to create an optimal wound dressing matrix. Additionally, PNM/PNMA NGs were functionalized with glycidyl methacrylate (GMA). The GMA contains an epoxide group, which is highly reactive and can undergo ring-opening reactions with nucleophiles such as amines, thiols, and hydroxyl groups. This reactivity allows GMA to act as a functionalization tool, enabling the introduction of additional chemical groups or the formation of covalent bonds within the nanogel structure [24]. The incorporation of GMA not only enhances the crosslinking of the gels and the encapsulation of bioactive molecules but also improves the mechanical strength of the hydrogel, thereby increasing its suitability for various applications [25,26].

Active natural compounds combined with suitable hydrogels have become an ideal solution for treating DFUs. Among natural compounds, paeoniflorin (PF), extracted from *Radix Paeoniae Rubra*, has shown pro-angiogenic, anti-inflammatory and antioxidant properties [27,28], as further confirmed by our network pharmacology and molecular docking analyses. Incorporating PF as a therapeutic agent into hydrogels enhances vascular remodeling and accelerates tissue repair, making it a promising candidate for DFUs treatment.

In this study, we aimed to develop a gel dressing that not only covers the wound but also exhibits excellent performance and enables controlled drug release. As illustrated in Scheme 1, poly(NIPAM-co-MAA) (PNM) and poly(NIPAM-co-MAA-co-MArg) (PNMA) nanogel particles (NGs) with dual-responsive properties were synthesized using MArg, NIPAM, and MAA. The most suitable hydrogel dressing was selected by systematic characterization of the materials. The therapeutic effect of PF on DFUs was initially verified through network pharmacology and molecular docking. In vitro and in vivo experiments demonstrated that PF@PNMA1 showed significant therapeutic effects in diabetic wound models. We hope that this experiment will not merely spark new innovations in biomaterial design but equally offer fresh perspectives for the treatment of DFUs.

2. Materials and methods

2.1. Materials

Reagents used in the study included L-arginine (>98 %, Aladdin Bio-Chem Technology Co., Shanghai), potassium carbonate (K_2CO_3, >99 %, Aladdin Bio-Chem Technology Co., Shanghai), acryloyl chloride (>96 %, Macklin Biochemical Co., Shanghai), anhydrous ether (>98 %, Damao Chemical Reagent Factory, Tianjin), paeoniflorin (PF, ≥98.0 %, Yuanye Bio-Technology Co., Shanghai). Sodium dodecyl sulfate (SDS, ≥99.0 %), *N*-isopropylacrylamide (NIPAM, ≥99.0 %), methacrylic acid (MAA, ≥99.0 %), ammonium persulfate (APS, ≥98.0 %), glycidyl methacrylate (GMA, ≥99.0 %), *N,N,N′,N′*-tetramethylethylenediamine (TEMED, ≥99.0 %), sodium hydroxide (NaOH, ≥97.0 %), and dialysis sacks with a molecular weight cutoff of 12,000 Da were purchased from Sigma-Aldrich. The water used was filtered and deionized using a Milli-Q® ultrapure water system.

2.2. Modification of L-Arginine

MArg was synthesized with reference to established protocols [29–31]. Acryloyl chloride served as the acylating agent, while K_2CO_3 was utilized to neutralize the hydrochloric acid generated during the reaction. A mixture of L-arginine (17.40 g, 0.10 mol) and potassium carbonate (14.80 g, 0.11 mol) was prepared in deionized water under N_2, and was cooled to 0 °C. Anhydrous ether (30 mL, 0.40 mol) was added, followed by dropwise addition of a mixture of acryloyl chloride (9 mL, 0.10 mol) and anhydrous ether (20 mL, 0.27 mol). The reaction was conducted at 0 °C for 3 h. Subsequent phase separation yielded an aqueous phase, which was adjusted to a pH of 7.4. This phase was washed with anhydrous ether, freeze-dried, and redissolved in methanol. After rotary evaporation, the solution was filtered and vacuum dried at 40 °C. The final product was stored at −20 °C.

2.3. Synthesis of PNM and PNMA NGs

In this study, PNM and PNMA NGs were synthesized through emulsion polymerization. SDS (0.80 g, 0.0028 mol) was introduced into a three-necked flask containing 160 g of water. The mixture was purged with N_2 and agitated for 15 min at 80 °C and 600 rpm. Then, NIPAM (2.5 g, 0.02 mol) was combined with MAA (7 g, 0.08 mol) to form solution A. Following the introduction of 0.22 g APS solution and 0.033 g TEMED, 2 mL of solution A was quickly added and allowed to react for 25 min. Different volumes of the MArg solution (0.50 g/mL) were mixed with the remaining solution A to form solution B. After 25 min, solution B was injected into the reaction system via a syringe pump at a rate of 0.17 mL/min, followed by stirring for 1 h. Dialysis was conducted for 7 d, with the water replaced twice daily.

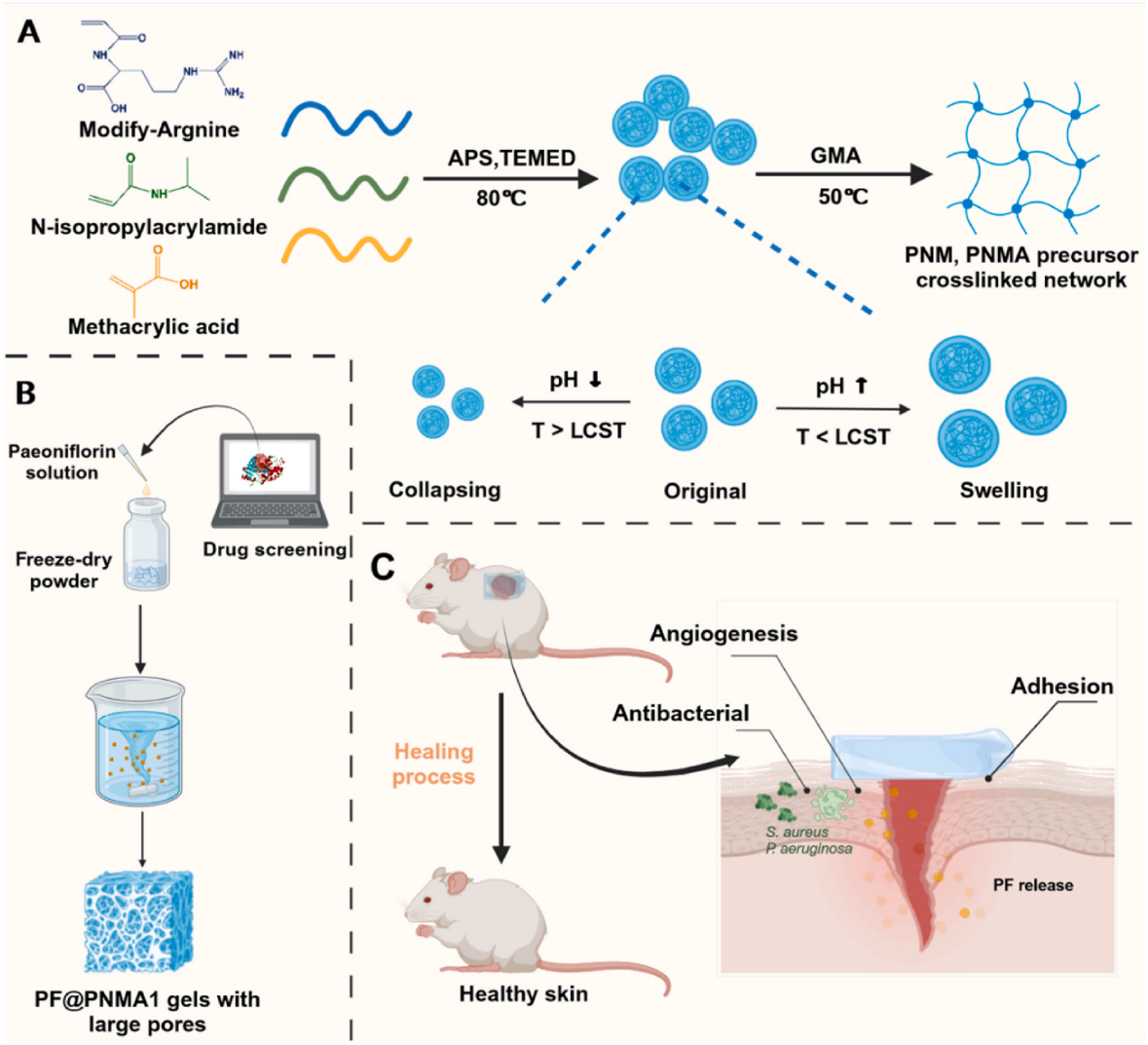

Scheme 1. Schematic of the design, synthesis, and applications of gels. **(A)** Synthesis of PNM/PNMA nanogel particles and their response to conditioned stimuli. **(B)** Virtual screening of PF and preparation of PF@PNMA1 gel. **(C)** Characterization of PF@PNMA1 gel and validation in animal models.

2.4. Preparation of GMA-functionalized PNM and PNMA NGs

The PNM and PNMA NGs solutions were concentrated to 10 wt% using rotary evaporation. The pH was adjusted to 7.4 with NaOH to ensure complete particle swelling. Subsequently, 0.06 mol of GMA was added to 50 g of PNM/PNMA NGs, and the mixture was purged with N_2 and stirred at 50 °C for 8 h. The process was followed by dialysis for an additional 3 days to remove residual impurities.

2.5. Preparation of PNM, PNMA, and PF@PNMA gels

For the preparation of PNM/PNMA gels, 5 wt% GMA-functionalized PNM and PNMA NGs were mixed with 2.5 % APS and heated in a water bath. PF-loaded PNM/PNMA (PF@PNM/PF@PNMA) gels were prepared by hybrid method. Briefly, PF dissolved in phosphate-buffered saline (PBS, pH 7.4) and added it to lyophilized GMA-functionalized PNM/PNMA NGs (EYELA FDU-2100, Japan). The remaining steps were carried out as previously described.

2.6. Physical measurements

2.6.1. Transmission electron microscopy (TEM) measurements

For morphological examination, 0.02 wt% dispersions of PNM and PNMA NGs were treated with an aqueous uranyl acetate solution and observed using TEM (FEI Tecnai G2 F30, USA).

2.6.2. Dynamic light scattering (DLS) measurements

The PNM and PNMA NGs dispersions were diluted to a concentration of 0.01 wt% using PBS solutions at various pH levels of 5.8, 6.5, 7, 7.4, 7.8, and 10.5. Particle sizes were subsequently measured at 25 and 37 °C using a Malvern Nano-ZS instrument (UK).

2.6.3. Scanning electron microscopy (SEM) measurements

After rapidly freezing the PNM and PNMA gels with liquid nitrogen and dried, their microstructure was observed using SEM (HITACHI SU8010, Japan).

2.6.4. Mechanical properties

The rheological behavior of the prepared PNM and PNMA gels was assessed using a temperature-controlled TA Instruments rheometer (DHR-2). Both storage (G′) and loss moduli (G″) were evaluated in the oscillation frequency mode across a frequency range of 0.1–100 rad/s with a constant strain of 1 %. Additionally, a strain amplitude sweep test was performed with the gels at a fixed frequency of 1 Hz (strain range: 0.1 %–500 %). A plate geometry with a diameter of 25 mm was employed for these tests.

2.6.5. Adhesion testing

Due to it similarities with human skin, porcine skin was chosen for the adhesion tests. The gel was hung upside down on the porcine skin and a certain load was applied to observe the behavior of the gel.

2.7. Antibacterial analyses

For this experiment, *Staphylococcus aureus* (*S. aureus*, ATCC 25923, 1×10^6 CFU/mL) was co-cultured with the appropriate hydrogels. After incubation, the cultures were harvested, appropriately diluted, and transferred to solid Luria-Bertani (LB) agar plates. The plates were incubated at 37 °C for 12 h, and the colony count was determined. Additionally, we evaluated the hydrogel's ability to inhibit Gram-negative bacteria, selecting *Pseudomonas aeruginosa* (*P. aeruginosa*) for this study.

2.8. In silico study of PF

The relevant targets of PF and DFUs were collected separately and analyzed using Cytoscape 3.10.0 software. Molecular docking was performed using Discovery Studio 2020 [32,33]. The detailed methods can be found in the Supplementary Material.

2.9. In vitro experiments

2.9.1. In vitro release of PF from gels

Solutions of PF were prepared at eight different concentrations to construct a standard curve. To assess PF release, the gel samples containing PF were immersed in 100 mL PBS (pH 7.4). A PF solution with an identical concentration served as the control solution and was subjected to the same procedure. Periodic 1 mL aliquots were removed from the solution at predetermined intervals and maintained at 37 °C. After each sampling event, an equivalent volume of PBS was added back into the solution to sustain a constant solution volume. UV–vis spectrophotometry was employed to measure the PF concentration at a wavelength of 230 nm. The concentration of the released PF was then determined based on the established standard curve.

2.9.2. Cytotoxicity assay, tube formation assay, and scratch wound-healing assay

L929 mouse fibroblast cells (Procell Life Science & Technology Co., Ltd.) were cultured in minimum essential medium (MEM) supplemented with non-essential amino acids, 10 % fetal bovine serum (FBS, Gibco), and 1 % penicillin/streptomycin (P/S, Gibco). HUVECs (ATCC) were maintained in DMEM enriched with 10 % FBS and 1 % P/S. Both cell types were incubated at 37 °C in a 5 % CO_2 environment.

To evaluate the effects of PF and materials on cell viability, MTT assays were conducted. L929 cells were seeded at a density of 3000 cells per well, and HUVECs were seeded at 5000 cells per well in 96-well plates. Following a 24 h incubation period, the cells were treated with various concentrations of PF (0, 100, 200, 300, 400, and 500 μM), PNMA1 (0, 200, 400, 600, 800, and 1000 μg mL^{-1}) and PF@PNMA1 (0, 100, 200, 300, 400, and 500 μM). After 24 h of incubation, the MTT reagent was added and the cells were incubated for an additional 4 h at 37 °C. The resultant formazan crystals were solubilized in 100 μL of dimethyl sulfoxide, and the absorbance was measured at 490 nm using a microplate reader.

Tube formation assays were employed to evaluate the influence of materials on neovascularization. Corning Matrigel® was thawed at 4 °C and dispensed into precooled 96-well plates (50 μL per well) using precooled tips. Following 30 min of gelation, complete medium and cell suspensions containing different concentrations of PF@PNMA1 (200, 500 μM) were gently added. After 4 h of incubation, the tube-like structures formed were observed and imaged under a microscope. The number of tube nodes and total branch lengths were quantified.

The scratch wound-healing assay was utilized as a classical in vitro model to assess cell migration. L929 cells were seeded in 6-well plates, and after reaching confluency to form a monolayer, a scratch was made using a 200 μL pipette tip. The plates were imaged under a light microscope (EVOS XL Imaging System, Thermo, US). After treating the cells with basal medium and PF@PNMA1 (200, 500 μM), the plates were incubated for 24 h. The extent of wound closure in each group was re-evaluated under a light microscope and photographed. ImageJ software was used to quantify the scratch areas before and after the assay.

2.10. In vivo wound healing experiment

The experimental procedure (**TCM-LAEC2023134**) was reviewed and approved by the Animal Ethics Committee of Tianjin University of Traditional Chinese Medicine. The experiments were conducted using SPF-grade healthy male SD rats weighing 200 ± 2 g. After being fed a high-fat diet for one week, the rats were fasted for 12 h and subsequently administered an intraperitoneal injection of 1 % STZ solution prepared with sodium citrate buffer at a dose of 50 mg/kg.

The SD rats were divided into five groups of six rats each: a control group, a blank preparation group (PNMA1), and three concentrations of PF@PNMA1 groups (200, 500 and 1000 μM). The rats were anaesthetized with isoflurane, and a 10 mm diameter full-thickness excisional wound was surgically created on their backs after shaving the area and disinfecting the skin with iodine. The control group wounds were covered with 3M Tegaderm®, the blank preparation group received PNMA1 gel without PF, and the three treatment groups received PNMA1 gel containing PF at 200, 500, and 1000 μM. Dressings were replaced every 48 h, and photographs of the wounds were taken on days 0, 2, 4, 6, 8, and 10 to monitor healing progress. Wound areas were measured using ImageJ software.

On day 10, the skin tissue surrounding the wounds was excised, rinsed with saline, and fixed in a paraformaldehyde solution. The fixed tissues were embedded in paraffin, sectioned, and subjected to histological analysis. Hematoxylin-eosin (HE) and Masson staining were performed to evaluate histomorphological changes, and tissue conditions were examined under a microscope. Additionally, the expression of CD31 in the tissue was analyzed using immunofluorescence staining.

2.11. Statistical analysis

All values were expressed as mean ± standard deviation (SD). Statistical significance was analyzed using one-way ANOVA with GraphPad Prism 8.0.1 software. Significance levels were set at $^*P < 0.05$, $^{**}P < 0.01$, $^{***}P < 0.001$, $^{****}P < 0.0001$ to discern statistically significant differences between groups. Nonsignificant results were denoted by ns.

3. Results and discussion

3.1. Synthesis and characterization of pH-Responsive and thermo-responsive PNM and PNMA NGs

In this study, arginine was successfully modified, and the structure of MArg as well as the results from Fourier transform infrared (FTIR) and ^{1}H NMR spectroscopy are presented in Fig. S1. PNM and PNMA NGs were synthesized using conventional emulsion polymerization methods. FTIR spectroscopy confirmed the successful synthesis of PNM and PNMA NGs (Fig. S2), while TEM was employed to analyze the morphology of the NGs, micrographs confirmed the spherical morphology of the synthesized NGs, as shown in Fig. 1A–D. Statistical analysis was performed on a sample of at least 100 NGs to evaluate their particle size distribution, revealing average particle sizes of 111, 124, 236, and 242 nm for PNM and PNMA NGs, respectively. The difference in particle size arises from the conditions under which NGs are prepared via emulsion polymerization. During particles formation, only a small amount of TEMED was added, ensuring that the initial particle sizes remained consistent across different systems. Ideally, during the phase separation stage,

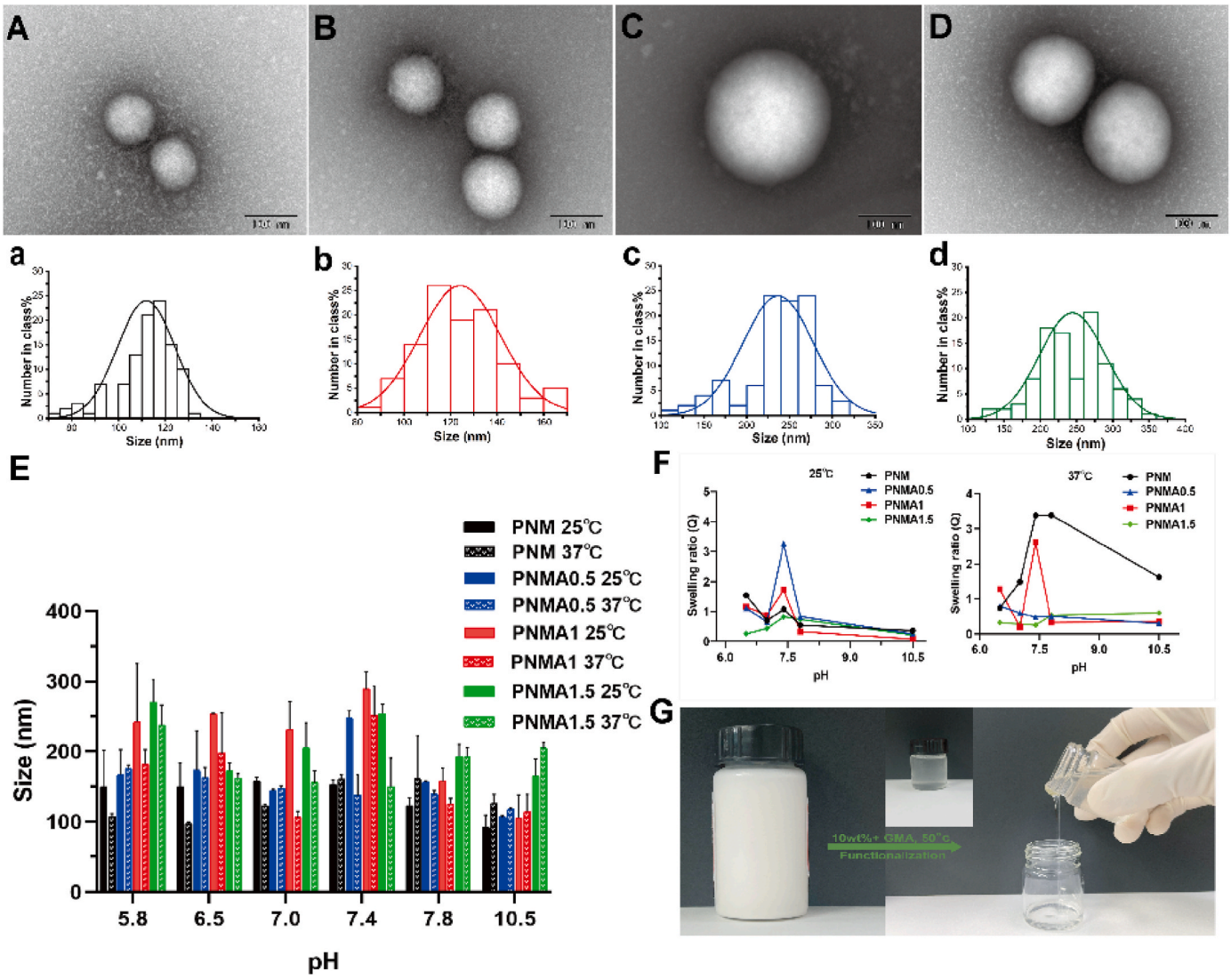

Fig. 1. TEM images of the**(A)** PNM, **(B)** PNMA0.5, **(C)** PNMA1, and **(D)** PNMA1.5 NGs and size distributions obtained by measuring at least 100 particles (from **a** to **d**). The scale bar is 100 nm. **(E)** Particle sizes variations of the PNM and PNMA systems at different pH and temperature values. **(F)** Swelling ratio (Q) of PNM and PNMA NGs at different pH and temperature values. **(G)** GMA functionalization.

polymer chains would contract through hydrophobic interactions to form a dense core. However, as the MArg concentration increased, the rapid formation of the crosslinked network hindered this contraction [34,35]. As a result, the network solidified before sufficient contraction could occur, leading to an increase in the final particle size.

Furthermore, the pH-responsive and thermo-responsive properties of PNM and PNMA NGs were evaluated via dynamic light scattering (DLS) measurements. Fig. 1E shows that the particle sizes of both PNM and PNMA systems exhibited variations depending on the pH value. A consistent trend was observed for different types of NGs: particle sizes increased as the pH value increased. In the case of PNMA1, for example, at pH 5.8, the particle diameter was 242 nm, indicating a collapsed state. When the pH value increased to 7.4, the particle diameter expanded to 289 nm. Zeta potential measurements were performed at pH values of 5.8 and 7.4 (Table 1). Increasing the pH resulted in a increase in the zeta potential due to the deprotonation of carboxyl groups, which enhanced the electrostatic repulsion between adjacent -COO^- groups. The lower critical solution temperature (LCST) of NIPAM is 32 °C; below this temperature, it adopts a hydrophilic unfolded conformation, while above the LCST, the conformation gradually shrinks due to the interaction of hydrophobic groups and intramolecular bonding. Consequently, particle sizes decrease at elevated temperatures. In addition,

Table 1
Properties of the PNM and PNMA nanoparticles.

Systems	d_{TEM} (nm)	$d_{pH\ 5.8}$(nm)	$d_{pH\ 7.4}$(nm)	$\varphi_{pH\ 5.8}$	$\varphi_{pH\ 7.4}$
PNM	111 ± 11	149	153	−4.04	−5.72
PNMA0.5	124 ± 12	167	248	−3.74	−7.28
PNMA1	236 ± 51	242	289	−4.07	−4.99
PNMA1.5	242 ± 41	273	254	−3.95	−6.56

a) dTEM represents the average particle sizes of NGs images obtained using TEM.
b) dpH 5.8/φpH 5.8 represent the average particle sizes and potential of NGs, respectively, determined using a laser scattering particle sizes analyzer at pH 5.8.
c) dpH 7.4/φpH 7.4 represent the average particle sizes and potential of NGs, respectively, determined using a laser scattering particle sizes analyzer at pH 7.4.

Fig. 1F illustrates the variation in the volume expansion ratio (Q) of the PNM and PNMA systems at different pH and temperature values, which partially reflects the responsiveness of the different systems. As the proportion of MArg increases to a certain level, the NGs stabilize, exhibiting reduced responsiveness to changes in environmental

conditions. The Q was determined using Equation: $Q=(d_{z(swell)}/d_{z(coll)})^3$. where $d_{z(swell)}$ denotes the d_z value in the swell condition and $d_{z(coll)}$ indicates the d_z value in the collapsed condition. Following GMA functionalization, the dispersion exhibited a transition to a more viscous state, as presented in Fig. 1G.

3.2. Morphology and mechanical properties of PNM and PNMA gels

Fig. S3 show that the crosslinking density between NGs increases with a higher proportion of MArg. This is because MArg provides a large number of amine groups, and an appropriate ratio can better facilitate the functionalization of NGs by GMA, forming a stable crosslinked structure. As further evidenced by the scanning electron microscopy (SEM) images (Fig. 2A and B), the PNM and PNMA gels exhibit a porous structure. The observed porosity results from highly swollen particles under pH 7.4 conditions, which after cross-linking and freeze-drying formed a porous matrix aligned along ice crystal growth pathways. Among the different gels, the PNMA1 gel exhibited the smallest and most uniform pore size (7.77 ± 2.20 μm) with a higher specific surface area. The increased specific surface area imparts the PNMA1 gel with a superior drug-carrying capacity.

The rheological properties of the PNM and PNMA gels prepared at 37 °C, and PNMA1 gel prepared at different temperatures were measured using a rheometer. As shown in Fig. 2C and D, the rheological results of the PNM and PNMA gels prepared at 37 °C showed that the storage modulus (G′) value was consistently greater than the loss modulus (G″) value, and the G′ value tended to decrease with increasing MArg concentration. Notably, a critical crossover point was observed when G′ decreased and G″ increased, identified as the critical strain (γ*). The γ* values for PNM, PNMA0.5, PNMA1, and PNMA1.5 were 55 %, 50 %, 63 %, and 58 %, respectively, with PNMA1 exhibiting the highest γ* value.

Subsequently, the PNMA1 gel was prepared at various temperatures. As shown in Fig. 2E and F, the rheological results of the PNMA1 gel showed that the G′ values tended to increase with increasing preparation temperature. The data presented in Fig. 2G indicate that the γ* values of gels at 37, 50, 60, and 80 °C were 63 %, 55 %, 60 %, and 53 %, respectively, with the highest γ* values obtained for the PNMA1 gel prepared at 37 °C. The γ* value is a parameter commonly used to assess the ductility of gels. As the γ* value increases, the gel is expected to become softer and more ductile. If the γ* of the gel is too low, it may easily fracture or detach under stretching or bending. Therefore, hydrogels intended for wound dressings require a relatively high γ* value. Compared to natural polymers such as fibrin and collagen (5 %–8

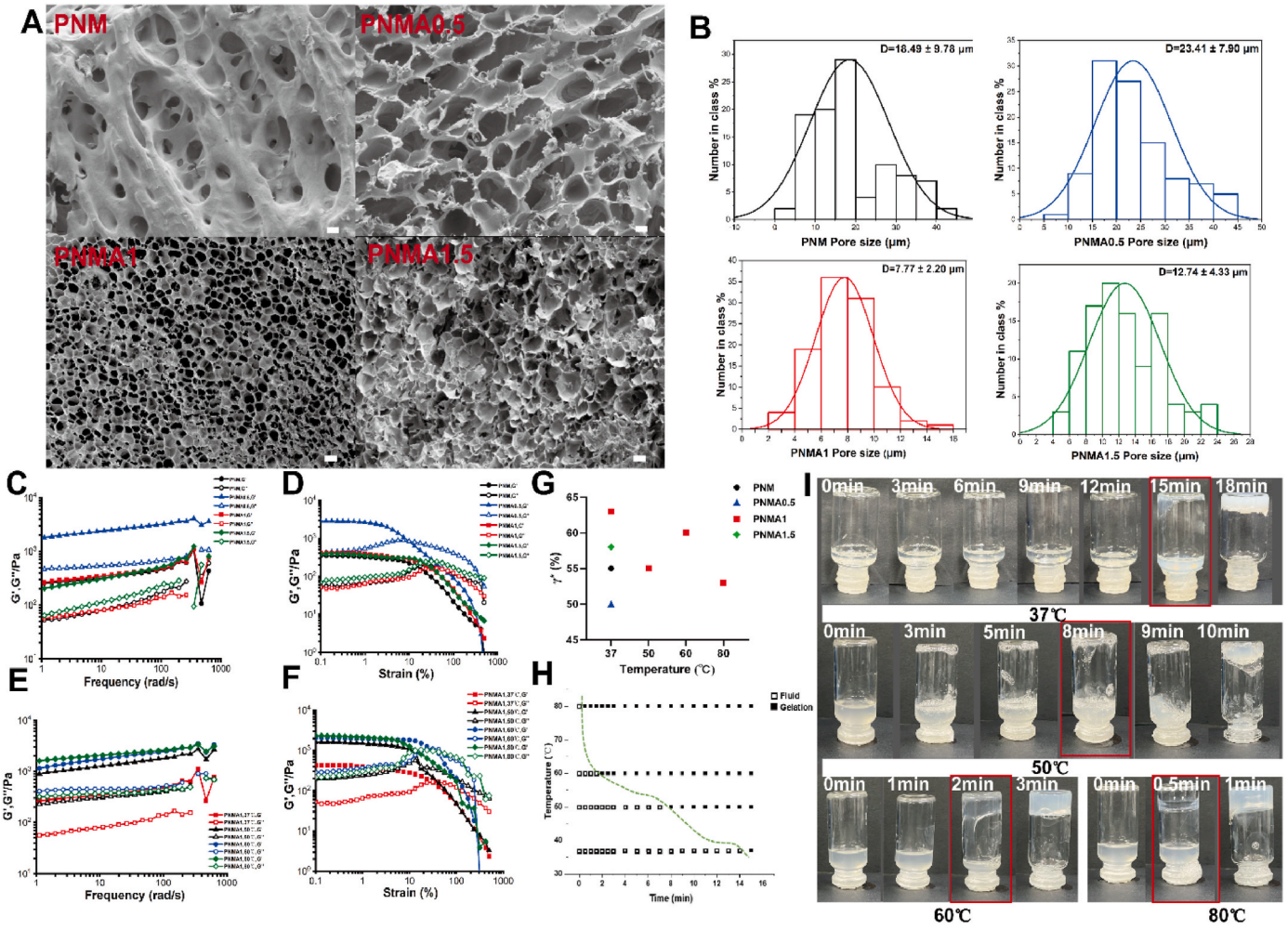

Fig. 2. **(A)** Scanning electron microscopy (SEM) images of freeze-dried PNM and PNMA gels at pH 7.4, 5 wt%, and 37 °C; The scale bar is 10 μm. **(B)** Statistical analysis of the pore sizes of the PNM and PNMA gels. **(C)** The frequency-sweep test was conducted at 1 % strain for the PNM and PNMA gels prepared at 37 °C. **(D)** The strain-sweep test was conducted at 1 Hz for the PNM and PNMA gels prepared at 37 °C. **(E)** The frequency-sweep test was conducted at 1 % strain for the PNMA1 gel prepared at different temperatures. **(F)** The strain-sweep test was conducted at 1 Hz for the PNMA1 gel prepared at different temperatures. **(G)** Critical strain (γ^*) for the PNM and PNMA gels under different conditions.
(H, I) Gelation time at different temperatures (Taking PNMA1 gel as an example, there is a consistent trend across different groups).

%) and synthetic polymers like boronate ester cross-linked 4-arm PEG (33.1 %–42.4 %) [36], the PNMA1 gel demonstrates a notably higher γ* value, making it more suitable for such applications.

As shown in Fig. 2H and I, in the case of PNMA1 gel, gelation occurs at a specific temperature. At higher temperatures, the gelation time decreases, but the resulting gels become more brittle. This is a result of the rapid contraction of NIPAM molecular chains with increasing temperature, leading to uneven distribution of crosslink density [37].

3.3. Antibacterial activity

According to the International Working Group on the Diabetic Foot (IWGDF) guidelines (2023 version) on the diagnosis and treatment of diabetic foot infections, *S. aureus* is the most common pathogen in DFUs infections [38]. Therefore, we investigated the antibacterial efficacy of the hydrogel against *S. aureus*. As shown in Fig. 3A and B, the PNM and PNMA gels were co-incubated in LB medium containing bacteria for a specified period, after which the resulting solution was diluted and plated for colony counting. After 3 h, the PNMA1 gel exhibited significant inhibition of *S. aureus* compared to the control. By 10 h, all experimental groups demonstrated significant antibacterial activity, showing significant inhibition relative to the control. This phenomenon may result from the hydrogels forms a physical barrier that hinders the propagation of bacteria. Consistently, the hydrogel formulation containing arginine exhibited excellent antibacterial efficacy, likely due to the intrinsic antibacterial properties of arginine [39]. To ensure a more comprehensive evaluation, we selected *P. aeruginosa* as a representative Gram-negative bacterium, as shown in Fig. S4. The hydrogel also demonstrated strong antibacterial activity against *P. aeruginosa*.

3.4. Gel adhesion ability testing

Porcine skin exhibits characteristics highly similar to human skin and is readily available. Therefore, we selected it to evaluate the adhesive properties of the hydrogels [40,41]. As shown in Fig. 3C, PNMA1 demonstrates strong adhesion to porcine skin, enabling it to support a certain amount of weight (the weight of porcine skin is 0.5 g). Hydrogels with enhanced ductility, softness, and skin adhesion help maintain a moist wound environment, reducing the likelihood of detachment.

Based on these results, the PNMA1 gel that was prepared at 37 °C with a solid content of 5 wt% at pH 7.4 was chosen as a carrier for the drug, and was used to further investigate its biological functions.

3.5. Selection of model drugs

The experiments described above have demonstrated that, among the various hydrogels, PNMA1 gel exhibits excellent mechanical properties, adhesion, and antibacterial activity, making it an ideal candidate for use as a wound dressing. Based on these promising results, we aimed to identify a model drug to combine with PNMA1 gel for the treatment of DFUs. PF has been shown to possess strong anti-inflammatory, antioxidant, and angiogenesis promoting properties, which are beneficial in addressing the pathological conditions of DFUs. To further investigate its therapeutic potential, we conducted network pharmacology and molecular docking studies, guided by a comprehensive review of the literature. These analyses revealed that PF has a strong binding affinity for DFUs related receptors and identified key gene functions and associated pathways (Figs. S5–8, Table S1).

3.6. In vitro PF release behavior

A standard curve was constructed to quantify the concentration of PF released (Fig. S9). PF from the control solution was rapidly released within 2 h, whereas PF release from the PF@PNMA1 gel followed a more sustained profile, extending continuously over 24 h. This difference in release behavior can be attributed to the high water-solubility of PF and

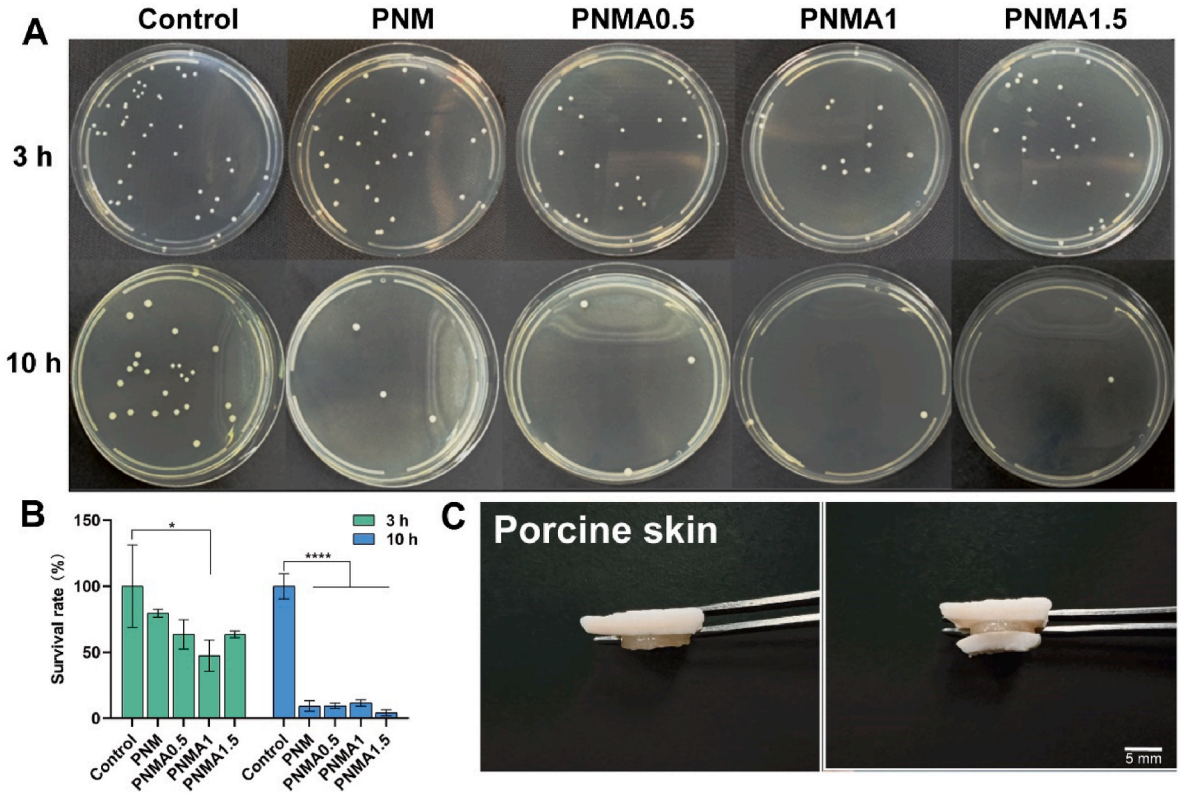

Fig. 3. **(A)** Inhibition of *S. aureus* by PNM and PNMA gels, photo of colonies of 3 h and 10 h. **(B)** Statistical analysis of colony data, $^{*}P < 0.05$, $^{****}P < 0.0001$. **(C)** Adhesion properties of the PNMA1 gel on porcine skin tissues. The scale bar is 5 mm.

the structural properties of the hydrogel. The dense polymer network of PNMA1 gels acts as a physical barrier to encapsulate the drug. This structure prevents PF from being immediately released into the medium, thus forcing it to gradually diffuse through the gel's pores [42]. Consequently, the release rate of PF is significantly prolonged. As illustrated in Fig. 4A, the release kinetics of PF from the PF@PNMA1 gel followed a first-order model, described by Equation: $M_t = 81.18(1-e^{-0.47t})$. Where t represents a specific point in time and M_t is the total amount released up to that point. The gradual release profile enhances the prolongation of drug action at the wound site, offering potential advantages for promoting wound healing.

3.7. Cell experiments

The cytotoxicity of the gels on L929 cells and HUVECs were evaluated using the MTT assay. As illustrated in Fig. 4B and C, PF, PNMA1, and PF@PNMA1 demonstrated excellent biocompatibility, exhibiting minimal cytotoxicity to L929 and HUVEC cells across a range of concentrations.

Neovascularization, a crucial factor in wound healing, was assessed through an in vitro HUVEC tube formation assay. The results demonstrated that the PF@PNMA1 at 200 μM significantly enhanced nodule formation ($^*P < 0.05$) and total tube length ($^{**}P < 0.01$) compared to the control group, indicating improved neovascularization at this concentration. In contrast, while PF@PNMA1 at 500 μM was non-cytotoxic to HUVECs, it did not significantly enhance tube formation (Fig. 4D–F). Additionally, as shown in Fig. 4G and H, PF@PNMA1 at 200 μM substantially promoted the migration of L929 cells, a key factor in the re-epithelialization process essential for wound healing. These results suggest that there is a need to optimize the concentration of PF in gel formulations to maximize therapeutic potential, which is also consistent with trends observed in other studies [43]. In conclusion, the findings suggest that PNMA1 and PF@PNMA1 demonstrate favorable safety profiles within an appropriate concentration range, making them promising candidates for wound dressing applications.

3.8. Promotion of diabetic wound healing

In this study, diabetic wound models in animals were successfully established (Fig. 5A). Rats were fasted for 12 h before intraperitoneal injection with streptozotocin (STZ). As shown in Fig. 5B, within one week of injection, the rats exhibited two random blood glucose values exceeding 16.7 mmol/L and displayed classic diabetic symptoms, including polydipsia, polyphagia, and polyuria, confirming the successful establishment of the diabetic model.

Fig. 5C and D illustrates the wound healing progress across different groups over 10 days. Both PNMA1 and PF@PNMA1 groups demonstrated significantly enhanced healing rates compared to the control group ($^{**}P < 0.01$ for the PF@PNMA1 200 μM group; $^*P < 0.05$ for the PNMA1, PF@PNMA1 500 μM, and PF@PNMA1 1000 μM groups). Notably, the PF@PNMA1 200 μM group also exhibited a significantly higher healing rate compared to the PNMA1 group ($^{**}P < 0.01$) and the PF@PNMA1 500 μM and 1000 μM groups ($^*P < 0.05$). However, no significant differences were observed between the PF@PNMA1 500 μM, 1000 μM groups and the PNMA1 group. These findings suggest that PNMA1 gel provides a therapeutic effect, and the addition of PF at 200

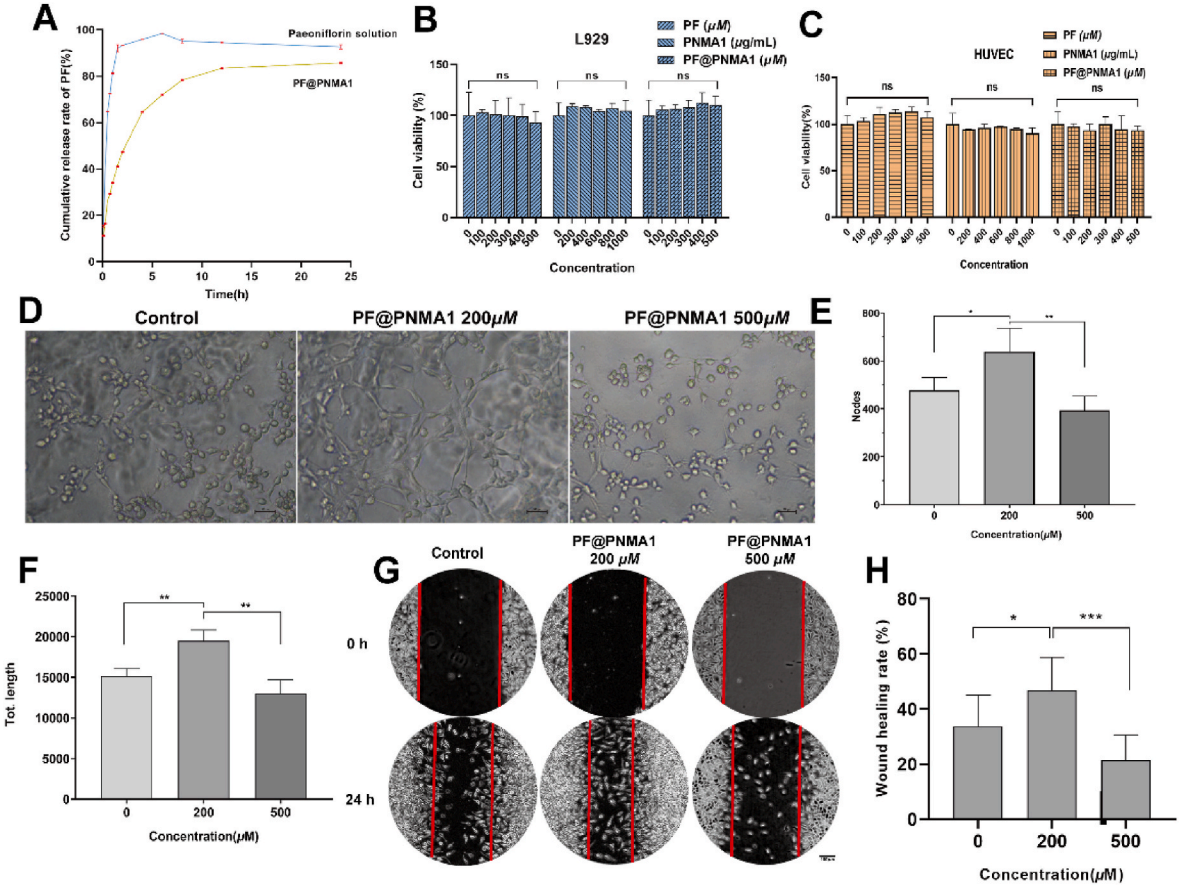

Fig. 4. Preliminary confirmation of PF for the treatment of DFUs and in vitro bioassay evaluation of the PNMA1 gel. **(A)** In vitro release of PF from PNMA1. **(B–C)** Effects of PF, PNMA1 and PF@PNMA1 on L929 cells and HUVECs, (ns, not significant). **(D)** HUVECs tube formation experiments. The scale bar is 100 μm. **(E–F)** Nodes and total length of HUVEC tube formation, $^*P < 0.05$, $^{**}P < 0.01$. **(G)** The wound healing of different formulations. The scale bar is 100 μm. **(H)** Wound healing rate of L929 cells, $^*P < 0.05$, $^{***}P < 0.001$.

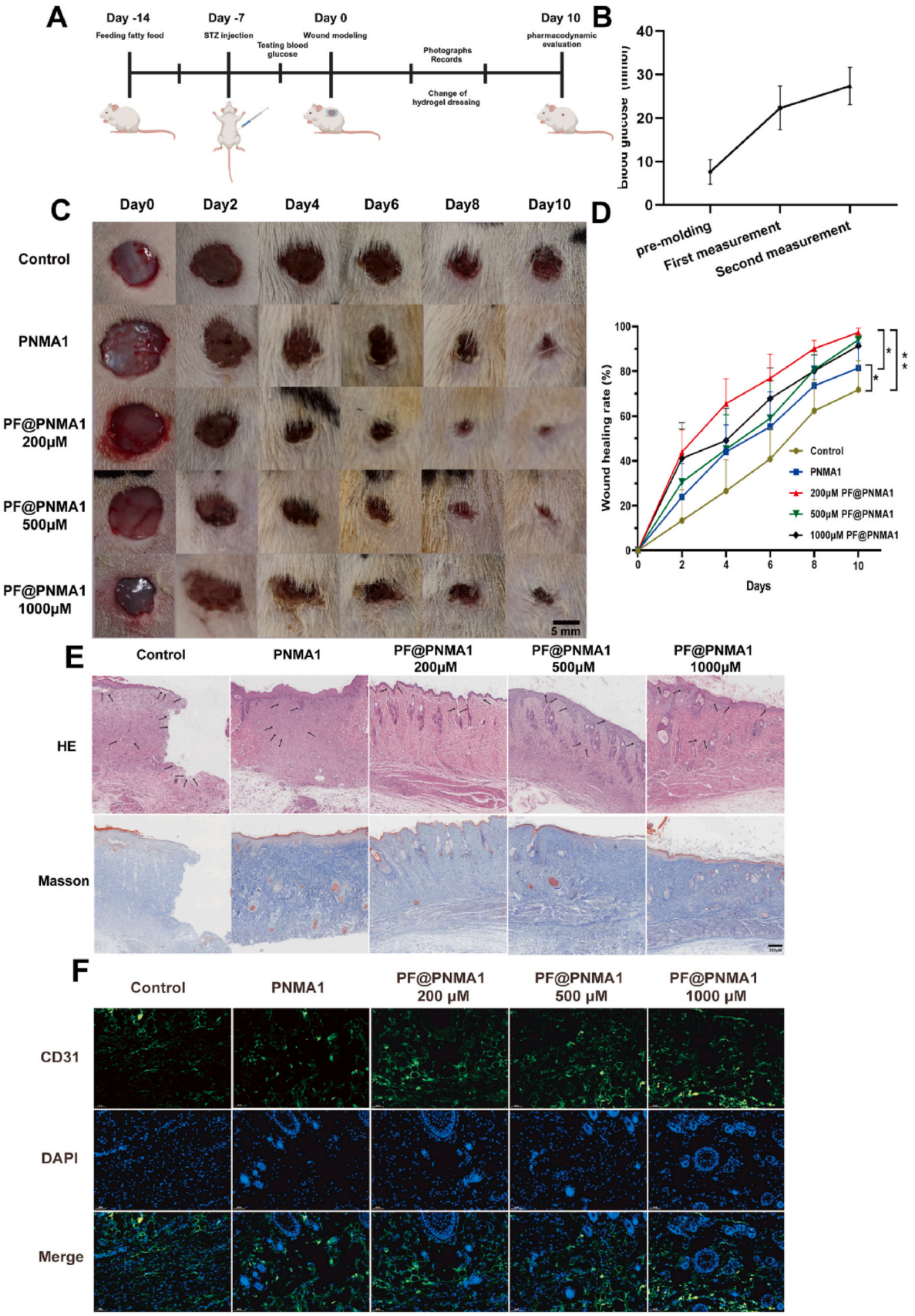

Fig. 5. **(A)** Animal model construction. **(B)** Blood glucose curve in SD rats after streptozotocin modeling. **(C)** Promotion of diabetic wound healing in rats by the control and PNMA1/PF@PNMA1 groups, recorded from wound images over 10 d. **(D)** Healing rate curve of diabetic wound in SD rats, $^{*}P < 0.05$, $^{**}P < 0.01$. **(E)** Results of HE and Masson staining. **(F)** Results of CD31 fluorescent staining.

μM synergistically accelerates wound healing by combining the benefits of the gels and the drug.

Hematoxylin-eosin (HE) staining revealed clear differences in tissue recovery among the groups. In the control group, wound healing was poor, with noticeable dermal tissue loss, pore damage, and a missing epidermal layer. The PNMA1 group showed dermal wounds and pore damage with mild inflammatory infiltration, but partial epidermal restoration was observed. In the PF@PNMA1 200 μM group, the skin tissue appeared nearly normal, with uniformly arranged pores and a fully restored epidermal layer. The PF@PNMA1 500 μM group exhibited visible skin regeneration with a relatively intact epidermis. However, the PF@PNMA1 1000 μM group showed signs of scarring, coarser pores, and relatively intact skin tissue. Masson staining highlighted the differences in collagen deposition among the groups. The control group exhibited fewer, irregularly arranged, and loosely packed collagen fibers. In contrast, PF-treated groups demonstrated deeper blue staining, indicating greater collagen fiber density and more organized arrangements (Fig. 5E). CD31, a marker expressed predominantly on endothelial cells of new blood vessels, was assessed to evaluate neovascularization [44]. Immuno-fluorescence analysis showed that the green fluorescence intensity in the PF@PNMA1 groups was higher than in the control and PNMA1 groups (Fig. 5F), indicating enhanced CD31 expression and superior tissue vascular regeneration.

These results collectively demonstrate that PF@PNMA1, particularly at a concentration of 200 μM, promotes more effective wound healing compared to the control group, driven by improved epidermal recovery, neovascularization and reduce tissue inflammation. In vivo studies have further confirmed that the incorporation of natural products with potent pharmacological activities into hydrogels has great potential for application.

4. Conclusion

In this study, we developed an amino acid-crosslinked hydrogel loaded with PF, which demonstrated superior mechanical strength, biocompatibility, antibacterial activity, and enhanced wound healing capacity in diabetic models. Our results indicated that increasing MArg content improved porosity, a key factor for drug loading and sustained release. The PNMA1 gel, prepared at 37 °C, exhibited good adaptability and softness, thereby reducing mechanical stress on tissues [45]. Compared to conventional dressings, PNMA1 gel showed superior moisture retention, essential for maintaining an optimal wound healing environment [46]. Additionally, its inhibition of *S. aureus* and *P. aeruginosa* suggests that amino acid modifications contribute to antibacterial activity, potentially reducing infection risks in chronic wounds. The therapeutic effects of PF may involve promoting tissue regeneration, enhancing angiogenesis, and regulating inflammation, consistent with previous reports [47,48]. The controlled release of PF from PNMA1 gel over 24 h maintained prolonged biological activity at the wound site, with optimal PF concentration enhancing its efficacy. In vivo experiments further confirmed the therapeutic benefits of PF@PNMA1. By day 10, the PF@PNMA1 200 μM group exhibited a 1.36-fold acceleration in wound healing speed compared to the control group, achieving a 97 % wound closure rate. Hydrogels incorporating natural amino acids and active compounds show promising potential.

However, limitations remain. The dual-responsive behavior of NGs requires further refinement to better adapt to dynamic wound environments, which could enable precise drug release and improved healing outcomes [49]. While preliminary biocompatibility tests have shown encouraging results, further studies are required to assess long-term safety, degradation behavior, and potential residual effects. In the future, multifunctional hydrogel dressings could serve as a powerful clinical tool for DFUs treatment or as a complementary therapy. Further research should focus on developing customizable formulations that adapt gel properties to individual wound conditions, thereby optimizing treatment efficacy. The groundbreaking results of this study highlight the immense potential of the PNMA1 gel as a novel material for wound healing applications, paving the way for innovative therapeutic strategies in regenerative medicine.

CRediT authorship contribution statement

Xintao Jia: Writing – review & editing, Writing – original draft, Visualization, Software, Investigation, Formal analysis, Data curation, Conceptualization. **Zixuan Dou:** Writing – review & editing, Writing – original draft, Visualization, Methodology, Conceptualization. **Ying Zhang:** Writing – review & editing, Writing – original draft, Project administration, Conceptualization. **Changxiang Yu:** Writing – review & editing, Writing – original draft, Resources. **Mengru Yang:** Visualization, Software. **Haonan Xie:** Writing – review & editing, Writing – original draft, Methodology, Investigation. **Yun Lin:** Writing – review & editing, Investigation. **Zhidong Liu:** Writing – review & editing, Writing – original draft, Visualization, Project administration, Investigation, Funding acquisition, Conceptualization.

Declaration of competing interest

The authors declare that they have no known competing financial interests or personal relationships that could have appeared to influence the work reported in this paper.

Acknowledgements

This work was supported by the National Administration of Traditional Chinese Medicine Young Qihuang Scholar Project and the Modern Traditional Chinese Medicine Haihe Laboratory Science and Technology Project (22HHZYSS00005).

We are also grateful for the help of the Instrumentation and Service Center for Physical Sciences, Westlake University and Animal Biosafety Level 2 (ABSL-2) Laboratory of Tianjin university of Traditional Chinese Medicine.

Appendix A. Supplementary data

Supplementary data to this article can be found online at https://doi.org/10.1016/j.mtbio.2025.101736.

Data availability

Data will be made available on request.

References

[1] G. Theocharidis, H. Yuk, H. Roh, L. Wang, I. Mezghani, J. Wu, A. Kafanas, M. Contreras, B. Sumpio, Z. Li, E. Wang, L. Chen, C. Guo, N. Jayaswal, X. Katopodi, N. Kalavros, C. Nabzdyk, I. Vlachos, A. Veves, X. Zhao, A strain-programmed patch for the healing of diabetic wounds, Nat Biomed Eng. 6 (10) (2022) 1118–1133.

[2] D.G. Armstrong, T.W. Tan, A.J.M. Boulton, S.A. Bus, Diabetic foot ulcers: a review, JAMA. 330 (1) (2023) 62–75.

[3] K. McDermott, M. Fang, A.J.M. Boulton, E. Selvin, C.W. Hicks, Etiology, epidemiology, and disparities in the burden of diabetic foot ulcers, Diabetes Care. 46 (1) (2023) 209–221.

[4] E.J. Boyko, L.R. Zelnick, B.H. Braffett, R. Pop-Busui, C.C. Cowie, G.M. Lorenzi, R. Gubitosi-Klug, B. Zinman, I.H. de Boer, Risk of foot ulcer and lower-extremity amputation among participants in the diabetes control and complications trial/epidemiology of diabetes interventions and complications study, Diabetes Care. 45 (2) (2022) 357–364.

[5] F. Huang, X. Lu, Y. Yang, Y. Yang, Y. Li, L. Kuai, B. Li, H. Dong, J. Shi, Microenvironment-based diabetic foot ulcer nanomedicine, Adv Sci (Weinh). 10 (2) (2023) e2203308.

[6] M. Hua, S. Wu, Y. Ma, Y. Zhao, Z. Chen, I. Frenkel, J. Strzalka, H. Zhou, X. Zhu, X. He, Strong tough hydrogels via the synergy of freeze-casting and salting out, Nature. 590 (7847) (2021) 594–599.

[7] P. Wu, L. Shen, H. Liu, X. Zou, J. Zhao, Y. Huang, Y. Zhu, Z. Li, C. Xu, L. Luo, Z. Luo, M. Wu, L. Cai, X. Li, Z. Wang, The marriage of immunomodulatory, angiogenic, and osteogenic capabilities in a piezoelectric hydrogel tissue engineering scaffold for military medicine, Mil Med Res. 10 (1) (2023) 35.

[8] F. Wang, Q. Sun, Y. Li, R. Xu, R. Li, D. Wu, R. Huang, Z. Yang, Y. Li, Hydrogel encapsulating wormwood essential oil with broad-spectrum antibacterial and immunomodulatory properties for infected diabetic wound healing, Adv Sci (Weinh). 11 (3) (2024) e2305078.
[9] R. Zeng, B. Lv, Z. Lin, X. Chu, Y. Xiong, S. Knoedler, F. Cao, C. Lin, L. Chen, C. Yu, J. Liao, W. Zhou, G. Dai, M. Shahbazi, B. Mi, G. Liu, Neddylation suppression by a macrophage membrane-coated nanoparticle promotes dual immunomodulatory repair of diabetic wounds, Bioact Mater. 34 (2024) 366–380.
[10] W. Xiao, X. Wan, L. Shi, M. Ye, Y. Zhang, S. Wang, A viscous-biofluid self-pumping organohydrogel dressing to accelerate diabetic wound healing, Adv Mater. (2024) e2401539.
[11] Y. Hao, S. Liu, S. Bingxue, C. Di, Y. Leilei, L. Meng, L. Huan, D. Yun, Y. Zhuo, G. Jianfeng, Modulation of macrophages by a paeoniflorin-loaded hyaluronic acid-based hydrogel promotes diabetic wound healing, Mater Today Bio. 12 (2021).
[12] X. Jia, Z. Dou, Y. Zhang, F. Li, B. Xing, Z. Hu, X. Li, Z. Liu, W. Yang, Z. Liu, Smart responsive and controlled-release hydrogels for chronic wound treatment, Pharmaceutics. 15 (12) (2023).
[13] Y. Wang, P. Katyal, J. Montclare, Protein-engineered functional materials, Adv Healthc Mater. 8 (11) (2019) e1801374.
[14] D. Griffin, M. Archang, C. Kuan, W. Weaver, J. Weinstein, A. Feng, A. Ruccia, E. Sideris, V. Ragkousis, J. Koh, M. Plikus, D. Di Carlo, T. Segura, P. Scumpia, Activating an adaptive immune response from a hydrogel scaffold imparts regenerative wound healing, Nat Mater. 20 (4) (2021) 560–569.
[15] D. Pranantyo, C. Yeo, Y. Wu, C. Fan, X. Xu, Y. Yip, M. Vos, S. Mahadevegowda, P. Lim, L. Yang, P. Hammond, D. Leavesley, N. Tan, M. Chan-Park, Hydrogel dressings with intrinsic antibiofilm and antioxidative dual functionalities accelerate infected diabetic wound healing, Nat Commun. 15 (1) (2024) 954.
[16] G. Mao, S. Tian, Y. Shi, J. Yang, H. Li, H. Tang, W. Yang, Preparation and evaluation of a novel alginate-arginine-zinc ion hydrogel film for skin wound healing, Carbohydr Polym. 311 (2023) 120757.
[17] M. Mirhaj, M. Tavakoli, J. Varshosaz, S. Labbaf, S. Salehi, A. Talebi, N. Kazemi, V. Haghighi, M. Alizadeh, Preparation of a biomimetic bi-layer chitosan wound dressing composed of A-PRF/sponge layer and L-arginine/nanofiber, Carbohydr Polym. 292 (2022) 119648.
[18] Y. Zhao, L. Luo, L. Huang, Y. Zhang, M. Tong, H. Pan, J. Shangguan, Q. Yao, S. Xu, H. Xu, In situ hydrogel capturing nitric oxide microbubbles accelerates the healing of diabetic foot, J Control Release. 350 (2022) 93–106.
[19] Y. Liang, M. Li, Y. Yang, L. Qiao, H. Xu, B. Guo, pH/glucose dual responsive metformin release hydrogel dressings with adhesion and self-healing via dual-dynamic bonding for athletic diabetic foot wound healing, ACS Nano. 16 (2) (2022) 3194–3207.
[20] F. Rothenhäusler, H. Ruckdaeschel, Amino acids as bio-based curing agents for epoxy resin: correlation of network structure and mechanical properties, Polymers. 15 (2) (2023).
[21] C. Shi, Y. Zhang, G. Wu, Z. Zhu, H. Zheng, X. Sun, Y. Heng, S. Pan, H. Xiu, J. Zhang, Z. Yin, Z. Yu, B. Liang, Hyaluronic acid-based reactive oxygen species-responsive multifunctional injectable hydrogel platform accelerating diabetic wound healing, Adv Healthc Mater. 13 (4) (2024) e2302626.
[22] Y. Lan, Y. Wang, X. Qi, E. Cai, Y. Xiang, X. Ge, H. Xu, X. Chen, Y. Li, Y. Shi, J. Shen, Z. Liao, A modified hyaluronic acid hydrogel with strong bacterial capture and killing capabilities for drug-resistant bacteria-infected diabetic wound healing, Int J Biol Macromol. 279 (Pt 3) (2024) 135301.
[23] H. Zhang, Y. Lu, L. Huang, P. Liu, J. Ni, T. Yang, Y. Li, Y. Zhong, X. He, X. Xia, J. Zhou, Scalable and versatile metal ion solidificated alginate hydrogel for skin wound infection therapy, Adv Healthc Mater. 13 (18) (2024) e2303688.
[24] A.I. Gugoasa, S. Racovita, S. Vasiliu, M. Popa, Grafted microparticles based on glycidyl methacrylate, hydroxyethyl methacrylate and sodium hyaluronate: synthesis, characterization, adsorption and release studies of metronidazole, Polymers. 14 (19) (2022).
[25] M. Rong, D. Liu, X. Xu, A. Li, Y. Bai, G. Yang, K. Liu, Z. Zhang, L. Wang, K. Wang, L. Lu, Y. Jiang, J. Liu, X. Zhang, A superparamagnetic composite hydrogel scaffold as in vivo dynamic monitorable theranostic platform for osteoarthritis regeneration, Adv Mater. 36 (35) (2024) e2405641.
[26] S. Meng, H. Hu, Y. Qiao, F. Wang, B.N. Zhang, D. Sun, L. Zhou, L. Zhao, L. Xie, H. Zhang, Q. Zhou, A versatile hydrogel with antibacterial and sequential drug-releasing capability for the programmable healing of infectious keratitis, ACS Nano. 17 (23) (2023) 24055–24069.
[27] L. Zhang, W. Wei, Anti-inflammatory and immunoregulatory effects of paeoniflorin and total glucosides of paeony, Pharmacol Ther. 207 (2020) 107452.
[28] J.P. Yadav, A. Verma, P. Pathak, A.R. Dwivedi, A.K. Singh, P. Kumar, H. Khalilullah, M. Jaremko, A.H. Emwas, D.K. Patel, Phytoconstituents as modulators of NF-κB signalling: investigating therapeutic potential for diabetic wound healing, Biomed Pharmacother. 177 (2024) 117058.
[29] Y. Kim, S. Binauld, M.H. Stenzel, Zwitterionic guanidine-based oligomers mimicking cell-penetrating peptides as a nontoxic alternative to cationic polymers to enhance the cellular uptake of micelles, Biomacromolecules. 13 (10) (2012) 3418–3426.
[30] D.Q. Wu, J. Zhu, H. Han, J.Z. Zhang, F.F. Wu, X.H. Qin, J.Y. Yu, Synthesis and characterization of arginine-NIPAAm hybrid hydrogel as wound dressing: in vitro and in vivo study, Acta Biomater. 65 (2018) 305–316.
[31] Z. Tianyang, Preparation and Properties of Amino Acid Based Drug Loaded Hydrogel Dressing, Jiangnan University, 2022.
[32] Y. Xiu, Z. Wu, Y. Chen, W. Mu, X. Zhao, M. Dong, Y. Li, Z. Bai, X. Xiao, Paeoniae Radix Alba effectively attenuates Polygonum multiflorum Thunb.-induced idiosyncratic liver injury by modulating M2 macrophage polarization, Acupunct Herb Med. 4 (2) (2024) 209–221.
[33] R. Mohd, Sultanat Shafiullah, Cytotoxicity of oleanane type triterpene from leaf extract of Pterospermum acerifolium (in vitro) and theoretical investigation of inhibitory signaling pathway, Chin Herb Med. 13 (1) (2020) 124–130.
[34] N. Nun, S. Hinrichs, M.A. Schroer, D. Sheyfer, G. Grübel, B. Fischer, Tuning the size of thermoresponsive poly(N-Isopropyl Acrylamide) grafted silica microgels, Gels 3 (3) (2017) 34.
[35] T. Kopač, A. Ručigaj, M. Krajnc, The mutual effect of the crosslinker and biopolymer concentration on the desired hydrogel properties, Int J Biol Macromol. 159 (2020) 557–569.
[36] E. Prince, Designing biomimetic strain-stiffening into synthetic hydrogels, Biomacromolecules. 25 (10) (2024) 6283–6295.
[37] H.G. Schild, Poly(N-isopropylacrylamide): experiment, theory and application, Prog Polym Sci. 17 (1992) 163–249.
[38] É. Senneville, Z. Albalawi, S.A. van Asten, Z.G. Abbas, G. Allison, J. Aragón-Sánchez, J.M. Embil, L.A. Lavery, M. Alhasan, O. Oz, I. Uçkay, V. Urbančič-Rovan, Z.R. Xu, E.J.G. Peters, IWGDF/IDSA guidelines on the diagnosis and treatment of diabetes-related foot infections (IWGDF/IDSA 2023), Clin Infect Dis. 79 (1) (2024) 286.
[39] H. Meltem, B. Mark, Polymers showing intrinsic antimicrobial activity, Chem Soc Rev. 51 (2022).
[40] Y. Chen, X. Guo, A. Mensah, Q. Wang, Q. Wei, Nature-inspired hydrogel network for efficient tissue-specific underwater adhesive, ACS Appl Mater Interfaces. 13 (50) (2021) 59761–59771.
[41] M. Suneetha, S. Zo, S.M. Choi, S.S. Han, Antibacterial, biocompatible, hemostatic, and tissue adhesive hydrogels based on fungal-derived carboxymethyl chitosan-reduced graphene oxide-polydopamine for wound healing applications, Int J Biol Macromol. 241 (2023) 124641.
[42] Q. Luo, Y. Yang, C. Ho, Z. Li, W. Chiu, A. Li, Y. Dai, W. Li, X. Zhang, Dynamic hydrogel-metal-organic framework system promotes bone regeneration in periodontitis through controlled drug delivery, J Nanobiotechnology. 22 (1) (2024) 287.
[43] H. Yang, L. Song, B. Sun, D. Chu, L. Yang, M. Li, H. Li, Y. Dai, Z. Yu, J. Guo, Modulation of macrophages by a paeoniflorin-loaded hyaluronic acid-based hydrogel promotes diabetic wound healing, Mater Today Bio. 12 (2021) 100139.
[44] B. Eunnyung, H. Ping, M.-G. Gaëlle, H. Dolores, S. Andrew Edward, N. Amy S, M. Nicholas, C. Cathleen R, G. Candece L, Integrin α3β1 promotes vessel formation of glioblastoma-associated endothelial cells through calcium-mediated macropinocytosis and lysosomal exocytosis, Nat Commun. 13 (2022).
[45] K. Fang, Q. Gu, M. Zeng, Z. Huang, H. Qiu, J. Miao, Y. Fang, Y. Zhao, Y. Xiao, T. Xu, R.P. Golodok, V.V. Savich, A.P. Ilyushchenko, F. Ai, D. Liu, R. Wang, Tannic acid-reinforced zwitterionic hydrogels with multi-functionalities for diabetic wound treatment, J Mater Chem B. 10 (22) (2022) 4142–4152.
[46] Z. Lan, R. Kar, M. Chwatko, E. Shoga, E. Cosgriff-Hernandez, High porosity PEG-based hydrogel foams with self-tuning moisture balance as chronic wound dressings, J Biomed Mater Res A. 111 (4) (2023) 465–477.
[47] J. Jiang, C. Dong, L. Zhai, J. Lou, J. Jin, S. Cheng, Z. Chen, X. Guo, D. Lin, J. Ding, W. Gao, Paeoniflorin suppresses TBHP-induced oxidative stress and apoptosis in human umbilical vein endothelial cells via the Nrf2/HO-1 signaling pathway and improves skin flap survival, Front Pharmacol. 12 (2021) 735530.
[48] X. Zhang, Y. Wu, H. Gong, Y. Xiong, Y. Chen, L. Li, B. Zhi, S. Lv, T. Peng, H. Zhang, A multifunctional herb-derived glycopeptide hydrogel for chronic wound healing, Small. 20 (36) (2024) e2400516.
[49] Y. Chen, X. Wang, S. Tao, Q. Wang, P.Q. Ma, Z.B. Li, Y.L. Wu, D.W. Li, Research advances in smart responsive-hydrogel dressings with potential clinical diabetic wound healing properties, Mil Med Res. 10 (1) (2023) 37.